Non-Equilibrium Properties of Semidilute Polymer Solutions under Shear Flow

2012 J. Phys.: Conf. Ser. 392 012003

(http://iopscience.iop.org/1742-6596/392/1/012003)

Journal of Physics: Conference Series **392** (2012) 012003 doi:10.1088/1742-6596/392/1/012003

Non-Equilibrium Properties of Semidilute Polymer Solutions under Shear Flow

Chien-Cheng Huang, Gerhard Gompper, and Roland G Winkler

Theoretical Soft Matter and Biophysics, Institute of Complex Systems and Institute for Advanced Simulation, Forschungszentrum Jülich, D-52428 Jülich, Germany

E-mail: r.winkler@fz-juelich.de

Abstract. We review results of the non-equilibrium properties of semidilute polymer solutions under shear flow. A hybrid simulation approach is adopted, combing molecular dynamics simulations and the multiparticle collision dynamics method, which has been shown to fully capture hydrodynamic interactions. The polymers exhibit a shear rate dependent deformation and alignment. In addition, shear thinning is observed, which is related to the finite polymer extensibility. It is characterized by the shear-rate dependent viscosity and the first normal-stress coefficient. The conformational and rheological properties are universal functions of a concentration dependent Weissenberg number. The cyclic dynamics of an individual polymer is described in terms of a shear-rate dependent tumbling time. The tumbling time is tightly linked to the polymer end-to-end vector relaxation time and depends on concentration, which is attributed to screening of hydrodynamic interactions in semidilute solutions.

1. Introduction

The properties of dilute polymer solutions under shear flow have been studied intensively [1–18]. Far less attention has been paid to the non-equilibrium properties of semidilute solutions [17–20]. Insight into the behavior of such systems is of fundamental importance in a wide spectrum of systems ranging from biological cells, where transport appears in dense environments, to turbulent drag reduction in fluid flow. While the dynamical behavior of polymers in dilute solution is strongly affected by hydrodynamic interactions [21–23], their relevance in semidilute solutions is less clear.

Experimental studies of single DNA molecules by fluorescence microscopy studies [1–4, 9] reveal a remarkably rich polymer dynamics in shear flow. A polymer chain exhibits large conformational changes and continuously undergoes stretching and compression cycles, denoted as tumbling, and never reaches a steady-state extension. The detailed temporal evolution depends upon the shear rate. These microscopic dynamical properties are tightly linked to the macroscopic rheological behavior of a polymer solution and give rise to phenomena such as shear-rate dependent viscosities and non-vanishing normal-stress differences [11, 16, 17, 21, 24, 25].

The characterization of the tumbling dynamics is an important step toward a microscopic understanding of the polymer dynamics, an issue which accordingly received considerable attention [2–4, 6–8, 10, 11, 18, 26–28]. As it turns out, this is a non-trivial task because of the non-Markovian nature of the process [4, 8, 11, 29]. As is commonly accepted by now, tumbling is a cyclic but non-periodic process, which poses challenges for the calculation of a characteristic time.

The complex interactions in polymer solutions hamper an analytical treatment. Here, computer simulations are essential to shed light on their rich and intricate dynamical behavior. We apply a hybrid mesoscale hydrodynamics simulation approach, which combines molecular dynamics simulations (MD) for the polymers with the multiparticle collision dynamics (MPC) method describing the solvent [22, 23, 30–36]. As has been shown, the MPC method is very well suited to study the non-equilibrium properties of polymers [12, 37–40], colloids [13, 41, 42], and other soft-matter object such as vesicles [43] and cells [44, 45] in flow fields. Moreover, simulation studies of the dynamics of polymers in dilute solution yield excellent agreement with predictions of the Zimm model [21, 33–35].

By this approach, we demonstrate that polymers in dilute and semidilute solutions exhibit large deformations and a strong alignment with the flow direction in simple shear flow [17, 18]. More importantly, in the stationary state, the *conformational* and *rheological properties* for various concentrations are universal functions of the Weissenberg number $\mathrm{Wi_c} = \dot{\gamma}\tau(c)$, where $\dot{\gamma}$ is the shear rate and $\tau(c)$ the concentration-dependent polymer end-to-end vector relaxation time at equilibrium. Hence, with increasing concentration, hydrodynamic interactions affect the conformational and rheological properties only via the increasing relaxation time $\tau(c)$. Experiments on DNA in shear flow [20] and simulations of polymer brushes [46] lead to a similar conclusion.

By analyzing the *non-equilibrium dynamical properties*—orientational distribution functions and tumbling times, which are extracted from gyration tensor correlation functions along the flow and gradient direction—of semidilute polymer solutions, we find that the dynamical behavior depends on concentration (in excess of $\tau(c)$), a dependence which we attribute to screening of hydrodynamic interactions in semidilute solution [18]. Compared to the dilute case, such a screening causes a broadening of orientational angle distribution functions and an increase of the tumbling frequency $f = \tau(c)/\tau_T$, where τ_T is the tumbling time, at the same Weissenberg number $\mathrm{Wi_c}$ in dilute and semidilute solutions. More importantly, the same asymptotic dependencies are obtained as function of the Weissenberg number $\mathrm{Wi_c}$ in dilute and semidilute solutions. This explains the previously obtained agreement between power spectral densities of free-draining and non-draining computer simulations [2].

In this article, we briefly review the results presented in Refs. [17, 18] for polymer conformational, rheological, and dynamical properties under shear flow of dilute and semidilute solutions, and discuss their connection in a coherent manner. In Sec. 2, the model and simulation approach are described. The conformational properties are discussed Sec. 3. Results for the rheological behavior are presented in Sec. 4. Sec. 5 addresses the dynamical aspects of polymers, including the tumbling dynamics, and Sec. 6 summarizes our findings.

2. Model and Parameters

We consider a solution of N_p linear flexible polymer chains embedded in an explicit solvent. Each polymer is comprised of N_m beads of mass M, which are connected by harmonic springs. The bond potential is

$$U_b = \frac{\kappa}{2} \sum_{i=1}^{N_m-1} \left(|\boldsymbol{R}_{i+1} - \boldsymbol{R}_i| - l\right)^2 , \tag{1}$$

where $\boldsymbol{R}_i$ denotes the position of monomer i, l is the bond length, and κ the spring constant. Inter- and intramolecular excluded-volume interactions are taken into account by the repulsive, shifted, and truncated Lennard-Jones potential

$$U_{LJ} = 4\epsilon \left[\left(\frac{\sigma}{r}\right)^{12} - \left(\frac{\sigma}{r}\right)^{6} + \frac{1}{4} \right] , \tag{2}$$

for $r < \sqrt[6]{2}\sigma$, where r is the distance between two monomers, and $U_{LJ} = 0$ for $r \geq \sqrt[6]{2}\sigma$. Here, ϵ characterizes the energy of the interaction potential and σ the diameter of a monomer. Newton's equations of motion for the polymer are integrated by the velocity Verlet algorithm with the time step h_p [47, 48].

The solvent is simulated by the multiparticle collision (MPC) dynamics method [22, 23, 30, 31]. It is composed of N_s point-like particles of mass m, which interact with each other by a stochastic process. The algorithm consists of alternating streaming and collision steps. In the streaming step, the particles move ballistically and their positions $\boldsymbol{r}_i$ are updated according to

$$\boldsymbol{r}_i(t+h) = \boldsymbol{r}_i(t) + h\boldsymbol{v}_i(t), \tag{3}$$

where $i = 1, \ldots, N_s$, h is the time interval between collisions—denoted as collision time—, and $\boldsymbol{v}_i$ is the velocity of particle i. In the collision steps, the particles are sorted into cubic cells of side length a and their relative velocities, with respect to the center-of-mass velocity

$$\boldsymbol{v}_{cm} = \frac{1}{N_c}\sum_{j=1}^{N_c}\boldsymbol{v}_j, \tag{4}$$

of the cell of particle i, are rotated around a randomly oriented axis by a fixed angle α, i.e.,

$$\boldsymbol{v}_i(t+h) = \boldsymbol{v}_i(t) + (\mathbf{R}(\alpha) - \mathbf{E})(\boldsymbol{v}_i(t) - \boldsymbol{v}_{cm}(t)), \tag{5}$$

where $\mathbf{R}(\alpha)$ is the rotation matrix, $\mathbf{E}$ is the unit matrix, and N_c is the total number of fluid particles in that cell.

The solvent-polymer coupling is achieved by taking the monomers into account in the collision step, i.e., for collision cells containing monomers, the center-of-mass velocity reads

$$\boldsymbol{v}_{cm}(t) = \frac{\sum_{i=1}^{N_c} m\boldsymbol{v}_i(t) + \sum_{j=1}^{N_c^m} M\boldsymbol{V}_j(t)}{mN_c + MN_c^m}, \tag{6}$$

where N_c^m is the number of monomers within the considered collision cell. To ensure Galilean invariance, a random shift is performed at every collision step [49]. The collision step is a stochastic process, where mass, momentum and energy are conserved, which leads to the build up of correlations between the particles and gives rise to hydrodynamic interactions.

To impose a shear flow, we apply Lees-Edwards boundary conditions [47, 50] for systems with short chains with $N_m = 50$. A local Maxwellian thermostat is used, which we denote as Maxwell-Boltzmann Scaling (MBS), to maintain the temperature of the fluid at the desired value [51]. A parallel MPC algorithm is exploited for systems of long chains, which is based on a three-dimensional domain-decomposition approach, where particles are sorted onto processors according to their spatial coordinates [17, 52]. Here, shear flow is imposed by the opposite movement of two confining walls. The walls are parallel to the xy-plane and periodic boundary conditions are applied in the x- and y-directions. The equations of motion of the solvent particles are modified by the wall interaction [50]. We impose no-slip boundary conditions by the bounce-back rule, i.e., the velocity of a fluid particle is reverted—in the reference moving with the wall—when it hits a wall, and phantom particles in a wall are taken into account. The same rule is applied for monomers when colliding with a wall [23].

We employ the parameters $\alpha = 130°$, $h/\sqrt{ma^2/(k_BT)} = 0.1$ (k_B is Boltzmann's constant and T is temperature), $\langle N_c\rangle = 10$, $M = m\langle N_c\rangle$, $l = \sigma = a$, $k_BT/\epsilon = 1$, $h/h_p = 50$, and the bond spring constant $\kappa = 5 \times 10^3 k_BT/a^2$. The latter choice ensures that the mean of the bond length changes by less than 0.5% and the variance of the bond length distribution by 3% only, even at

the largest shear rate. Transport properties of the solvent depend on h, α, $\langle N_c \rangle$ [23, 50]. Tuning these variables allows us to attain solvents with a high Schmidt number and low Reynolds number, where momentum transport dominates over mass transport. The above parameters correspond to the solvent viscosity $\eta = 8.7\sqrt{mk_BT/a^4}$ and a Schmidt number $Sc = 17$. The polymer lengths $N_m = 50$ and 250 are considered in the concentration ranges $c/c^* = 0.16 - 2.08$ and $0.17 - 10.38$, respectively, and for the shear rates $\dot{\gamma}/\sqrt{k_BT/(ma^2)} = 10^{-4} - 3 \times 10^{-1}$ and $\dot{\gamma}/\sqrt{k_BT/(ma^2)} = 10^{-6} - 3 \times 10^{-2}$, respectively. The corresponding overlap concentrations are $c^* = 0.098l^3$ and $c^* = 0.029l^3$, determined by their radii of gyration. In dilute solution, the equilibrium end-to-end vector relaxation times are $\tau_0/\sqrt{ma^2/(k_BT)} = 6169$ and 78330 [17]. Brownian MPC simulations [23, 53]—where hydrodynamic correlations are switched off—yield an approximately five times larger relaxation time than hydrodynamic MPC for $N_m = 50$.

A posteriori, knowing the non-equilibrium behavior of the polymer, it can be demonstrated that the Reynolds number Re for the polymer is smaller than unity. The radius of gyration tensor of a polymer chain is defined as

$$G_{\beta\beta'} = \frac{1}{N_m} \sum_{i=1}^{N_m} \langle \Delta r_{i,\beta} \Delta r_{i,\beta'} \rangle, \tag{7}$$

where $\Delta r_{i,\beta}$ is the position of monomer i in the center-of-mass reference frame of the polymer ($\beta, \beta' \in \{x, y, z\}$) [17]. Using its $y-$component G_{yy} as characteristic length scale, the Reynolds number Re is given by $Re = v\sqrt{G_{yy}}/\nu$, where $\nu = \eta/(m\langle N_c \rangle)$ is the kinematic viscosity of our MPC solvent. Shear implies a rotation of the fluid and the polymer with the frequency $\omega_R = \dot{\gamma}/2$ at low shear rates. Hence, we set $v = \omega_R\sqrt{G_{yy}} = \mathrm{Wi_c}\sqrt{G_{yy}}/(2\tau(c))$, which yields

$$Re = \frac{\mathrm{Wi_c} G_{yy}}{2\tau(c)\nu}. \tag{8}$$

At low Weissenberg numbers $\mathrm{Wi_c} \lesssim 10$, the conformations of a polymer are little perturbed compared to the equilibrium state, hence, $G_{yy} \approx R_{g0}^2$, where R_{g0}^2 is equilibrium radius of gyration in dilute solution. For the polymer lengths $N_m = 50$ and $N_m = 250$, $R_{g0}^2 = 24.5l^2$ and $R_{g0}^2 = 163.5l^2$, respectively, as documented in Ref. [17]. With the above relaxation times τ_0, this yields $Re < 0.1$ for $\mathrm{Wi_c} < 50$. For larger Weissenberg numbers, we take into account the deformation of the radius of gyration tensor. As shown in Ref. [17], G_{yy} decreases for $\mathrm{Wi_c} > 50$ approximately as $G_{yy} \sim 1/\sqrt{\mathrm{Wi_c}}$. With $G_{yy} \approx R_{g0}^2/\sqrt{\mathrm{Wi_c}}$, we find $Re < 0.2$ up to $\mathrm{Wi_c} = 10^4$. The applied approximations certainly overestimate the Reynolds number, since the frequency ω_R also depends on the Weissenberg number for $\mathrm{Wi_c} > 1$ and increases slower than linear with $\mathrm{Wi_c}$, as has been shown for star polymers in Refs. [13, 53].

3. Conformations

We characterized the flow strength by the Weissenberg number $\mathrm{Wi_c} = \dot{\gamma}\tau(c)$, i.e., by the concentration dependent relaxation time. In the weak-shear flow regime, with $\mathrm{Wi_c} \ll 1$, the chains are able to undergo conformational changes before the local strain has changed by a detectable amount, while in the strong shear-flow regime $\mathrm{Wi_c} \gg 1$, the chains are driven by the flow and they are not able to relax back to the equilibrium conformation. This is illustrated in Fig. 1, which displays snapshots for various flow rates. At small $\mathrm{Wi_c}$, the polymers are only weakly perturbed and are close to their equilibrium conformations, whereas large $\mathrm{Wi_c}$ imply large deformations and a strong alignment with flow. The question is, to what extent the influence of concentration on the polymer dynamics can be accounted for by a concentration-dependent Weissenberg number. As we will see, this concept applies well for all structural and rheological properties.

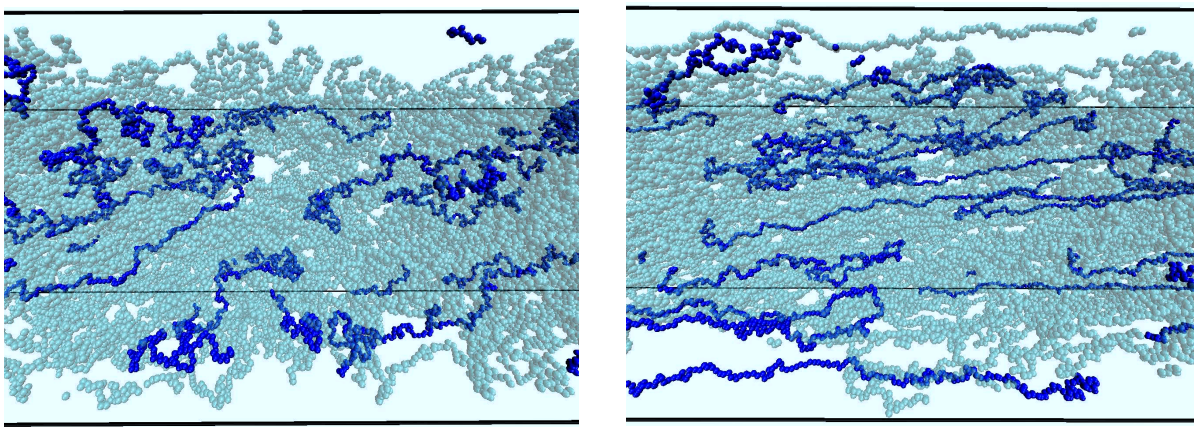

Figure 1. Snapshots of systems with $N_p = 400$ polymers of length $N_m = 250$ for the Weissenberg numbers $\mathrm{Wi_c} = 13$ (left) and $\mathrm{Wi_c} = 126$ (right). For illustration, some of the chains are highlighted in red.

The polymer deformation is quantified by the gyration tensor (7). In Fig. 2, the relative deformation along the flow direction

$$\delta G_{xx} = \frac{G_{xx} - G^0_{xx}}{G^0_{xx}}, \tag{9}$$

where $G^0_{xx} = R_g^2/3$ is the gyration tensor component and R_g^2 the radius of gyration at equilibrium for the particular concentration, is shown for various concentrations and polymer lengths. A significant polymer stretching appears for $\mathrm{Wi}_c > 1$. At large shear rates, the stretching saturates at a value smaller than the value corresponding to a fully stretched chain ($G_{xx} \approx l^2 N_m^2/12$) and reflects the finite size of a polymer. This is consistent with experiments on DNA [2, 9], where the maximum extension is on the order of half of the contour length, and theoretical calculations [16]. It is caused by the large conformational changes of the polymers during the tumbling cycles, which yields an average extension smaller than the contour length. Nevertheless, molecules assume totally stretched conformations at large Weissenberg numbers during their tumbling dynamics. Interestingly, a universal dependence is obtained for δG_{xx} as function of a concentration-dependent Weissenberg number Wi_c at a given polymer length. In contrast, polymers at larger concentrations exhibit a stronger stretching in terms of the Weissenberg number $\mathrm{Wi} = \dot\gamma \tau_0$ for a dilute solution, because their actual concentration dependent relaxation time is larger and hence their Weissenberg number is higher.

Theoretical calculations for single polymers in dilute solution predict the dependence $\delta G_{xx} = C_x \mathrm{Wi}^2$ for $\mathrm{Wi} < 1$, where C_x is a universal constant. The renormalization group calculations of Ref. [15] yield $C_x = 0.27$, whereas a calculation based on a Gaussian phantom chain model yields $C_x \approx 0.3$ [11, 16, 54–56]. As shown in Fig. 2, the simulations confirm the quadratic dependence on the shear rate; δG_{xx} is independent of chain length for $\mathrm{Wi} < 1$ and $C_x \approx 0.1$. For $\mathrm{Wi} > 10$, finite-size effects appear and different asymptotic values are assumed for the two chain lengths. We like to stress that our simulations are in agreement with the molecular dynamics simulation results of Ref. [56] and the SANS data of Refs. [57, 58].

As is evident from the average shape of an individual chain displayed in Fig. 3, a polymer is not only stretched by the flow, but also aligned. This alignment is characterized by the angle χ_G, which is the angle between the eigenvector of the gyration tensor with the largest eigenvalue

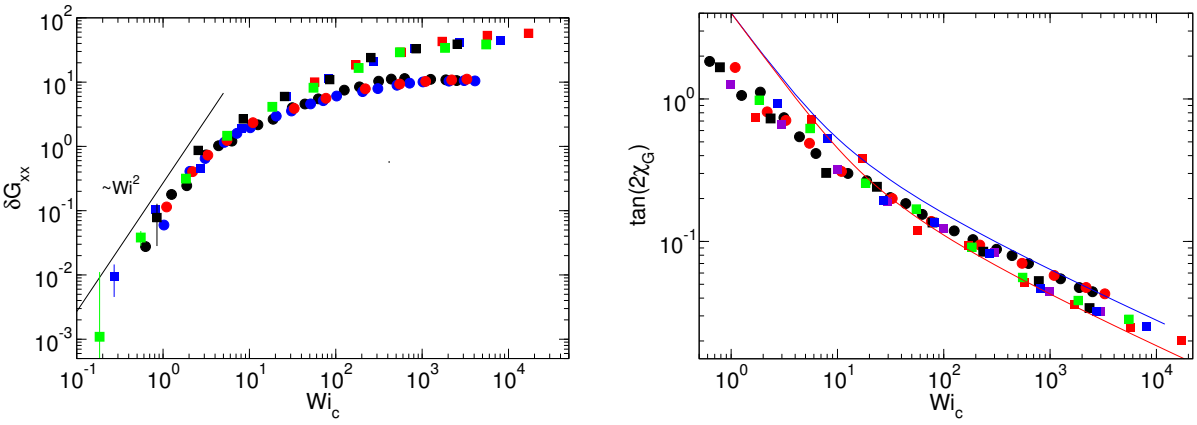

Figure 2. Deformation ratios δG_{xx} (left) and $\tan(2\chi_G)$ (right) as function of Weissenberg number. Bullets correspond to systems with $N_m = 50$ for $c/c^* = 0.16$ (●), $c/c^* = 1.6$ (●), and $c/c^* = 2.08$ (●). Squares denote results for $N_m = 250$ with the concentrations $c/c^* = 0.17$ (■), $c/c^* = 2.77$ (■), $c/c^* = 5.19$ (■), and $c/c^* = 10.38$ (■). The line in δG_{xx} indicates the dependence $\delta G_{xx} \sim \mathrm{Wi}^2$, and the lines for $\tan(2\chi_G)$ are theoretical results according to Refs. [11, 16] for $N_m = 50$ (blue) and $N_m = 250$ (red).

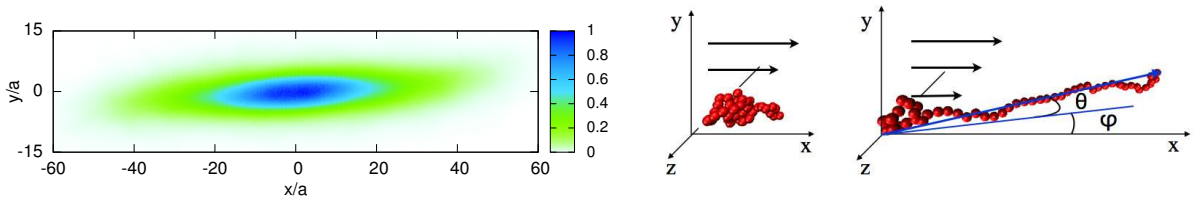

Figure 3. Monomer density distribution in the flow-gradient plane for $N_m = 250$, $c/c^* = 10.38$, and $\mathrm{Wi_c} = 569$ (left). Illustration of polymer stretching and recoiling and the definition of the angles θ and φ (right). θ is the angle between the end-to-end vector and its projection onto the flow-gradient plane and φ is the angle between this projection and the flow direction.

and the flow direction. It is obtained from the components of the radius of gyration tensor via

$$\tan(2\chi_G) = \frac{2G_{xy}}{G_{xx} - G_{yy}}. \tag{10}$$

The dependence of $\tan(2\chi_G)$ on shear rate and concentration is shown in Fig. 2. Again, a universal curve is obtained for the different concentrations at a given polymer length. Moreover, $\tan(2\chi_G)$ seems to be independent of polymer length for $\mathrm{Wi_c} < 100$, whereas we find a length dependence for larger Weissenberg numbers. In this high shear-rate regime, we find $\tan(2\chi_G) \sim (\mathrm{Wi}_c)^{-1/3}$. We like to emphasize that only the shear rate can be scaled in order to arrive at a universal function. The angle, or $\tan(2\chi_G)$, cannot be scaled to absorb flow or polymer properties in an effective variable. Hence, the universal behavior of the alignment angle for various concentrations confirms that the Weissenberg number Wi_c is the correct scaling variable and that the alignment of polymers at different concentrations depends on the combination $\mathrm{Wi_c} = \dot{\gamma}\tau_c$ of shear rate and relaxation time only.

The analytical approach of Refs. [11, 16] predicts the dependence

$$\tan(2\chi_G) \sim \left(\frac{l_p}{L\mathrm{Wi}^*}\right)^{1/3} \tag{11}$$

for semiflexible polymers in dilute solution in the limit $\mathrm{Wi}^* \to \infty$. Here, we introduce the Weissenberg number $\mathrm{Wi}^* = \dot{\gamma}\tau_{\mathrm{th}}$ for the theoretical result, because the relaxation times from theory and simulation might not be exactly the same; L is the length and l_p the persistence length of the polymer. The analytical result describes the simulation data well at large shear rates, when the Weissenberg number of the theoretical model is set to $\mathrm{Wi}^* = \mathrm{Wi}_c/2$. To compare the predicted length dependence with that of the simulation, we apply the relation $\langle R_e^2\rangle = 2l_pL$ to obtain a persistence length, with $\langle R_e^2\rangle$ the polymer mean square end-to-end distance in dilute solution at equilibrium, which yields $l_p/L \approx 0.025$ for $N_m = 50$ and $l_p/L \approx 0.008$ for $N_m = 250$. With these values, the ratio of $\tan(2\chi_G)$ of the polymer of length $L = 50a$ and $L = 250a$ is 1.5. This compares well with the factor 1.33 following from the simulation results, which suggests that excluded-volume interactions are of minor importance for intermediate flow rates.

In the limit $\mathrm{Wi}_c \to 0$, theory predicts $\tan(2\chi_G) \sim \mathrm{Wi}_c^{-1}$. The simulation data do not show this dependence on the considered range of Weissenberg numbers, which might be due to excluded-volume interactions.

4. Rheology

Applying a shear flow, the viscosity $\eta(\dot{\gamma})$ is obtained from the relation

$$\eta(\dot{\gamma}) = \frac{\sigma_{xy}(\dot{\gamma})}{\dot{\gamma}}, \tag{12}$$

where σ_{xy} is the shear stress [24, 59]. In our simulations, σ_{xy} is calculated using the virial formulation of the stress tensor [47, 50, 60]. For sufficiently weak flow, the polymer solution is in the Newtonian regime, i.e., $\sigma_{xy} \sim \dot{\gamma}$ and the viscosity is independent of shear rate. Thus, the viscosity obtained in this low shear rate regime is equal to the zero-shear viscosity denoted by η_0. A discussion of concentration dependence of η_0 can be found Ref. [17].

At sufficiently large shear rates, the polymers are aligned and deformed, which implies shear thinning [11, 14, 16, 24]. Figure 4 shows the polymer contribution η^p to the shear viscosity. Similar to the alignment angle, the viscosity is a universal function of the Weissenberg number Wi_c and shows a weak dependence on polymer length. It is independent of shear rate for $\mathrm{Wi}_c \ll 1$, decrease approximately as $\mathrm{Wi}_c^{-0.3}$ for $1 < \mathrm{Wi}_c < 10^2$, and $\mathrm{Wi}_c^{-0.45}$ for higher shear rates. This behavior is consistent with other simulation results [9, 46, 61–63]. However, an even stronger decay of the viscosity is observed in simulations at larger shear rates in Refs. [9, 14]. Experiments of dilute polymer solutions reported exponents ranging from -0.4 to -0.85 [9, 24]. Theoretical calculations for dumbbells and finite extensible polymers predict the dependence $\eta_p \sim \mathrm{Wi}^{-2/3}$ in the limit $\mathrm{Wi} \to \infty$ [11, 16, 24, 25, 64]. The differences in the observed behavior can be explained by a broad crossover regime before the asymptotic behavior is reached, as suggested by the simulations of Ref. [9]

The ratio of the viscosities of the two lengths is approximately 1.33 for the large Weissenberg-number regime, as for the alignment angle, which compares well with the theoretically predicted length dependence in Eq. (11).

The concentration and shear-rate dependencies of the first normal-stress coefficient [24, 25]

$$\Psi_1 = (\sigma_{xx} - \sigma_{yy})/\dot{\gamma}^2 \tag{13}$$

is displayed in Fig. 4. Within the accuracy of the simulations, the ratio Ψ_1/Ψ_1^0, where Ψ_1^0 is the stress coefficient at zero shear rate, is a universal function of Wi_c for various concentrations and

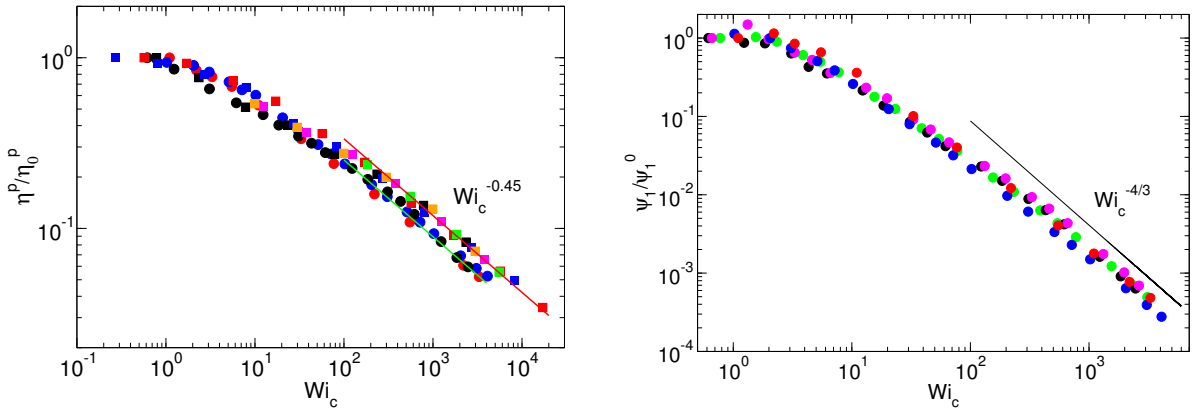

Figure 4. Polymer contribution η_p to the shear viscosity (left) and first normal-stress coefficient Ψ_1 (right) as function of shear rate. Bullets correspond to systems with $N_m = 50$ for $c/c^* = 0.16$ (●), $c/c^* = 0.41$ (●), $c/c^* = 0.81$ (●), $c/c^* = 1.63$ (●) and $c/c^* = 2.08$ (●). Squares denote results for $N_m = 250$ with the concentration $c/c^* = 0.17$ (■), $c/c^* = 0.35$ (■), $c/c^* = 1.38$ (■), $c/c^* = 2.77$ (■), $c/c^* = 5.19$ (■), and $c/c^* = 10.38$ (■).

decreases as $\Psi_1 \sim \dot{\gamma}^{-4/3}$ for large shear rates. This is consistent with analytical calculations [16, 24, 25], various computer simulations [9, 17, 25, 61–63, 65], and experiments [2, 3] for dilute solutions. Similar to the viscosity, the decay is related to the finite polymer extensibility.

Surprisingly, the first normal-stress coefficient follows the theoretical prediction [16, 24, 25] already for moderate Weissenberg numbers, whereas the viscosity η^p does not. This is consistently found in various simulation studies applying different models and simulation approaches [9, 17, 25, 61–63, 65]. The origin of the disparity is not clear. Theoretical models based on phantom polymers, i.e., models neglecting excluded-volume interactions, suggest an intimate coupling of the shear-rate dependence of the viscosity and the normal-stress coefficient [16]. It seems that excluded-volume interactions, which lead to a tight coupling of the polymer deformation along the flow and gradient direction, as expressed in the correlation function presented in Fig. 6 (left), affect the shear stress σ_{xy} more severely and lead to the observed differences. Such a coupling is not captured in a phantom chain model. This speculation could be checked by simulations of phantom chains.

5. Angular Probability Distribution Functions

The probability distribution function (PDF) $P(\varphi)$ for the orientation angle φ (for a definition of φ, see Fig. 3 (right)) provides further insight into the orientational behavior of polymers [4, 6, 8, 11]. Theoretical calculations yield the expression [11]

$$P(\varphi) = \frac{\sqrt{\pi^4 + 4\mathrm{Wi}^{*2}(\pi^2-4)/\mu^2}}{2\pi\left[\pi^2+4\right]\mathrm{Wi}^{*2}\sin^2(\varphi)/\mu^2 - 4\mathrm{Wi}^*\sin(2\varphi)/\mu} \tag{14}$$

in the limit of long and flexible polymers $L/l_p \gg 1$, where μ follows from the equation

$$\mu^3 - \mu^{5/2} - \frac{\pi^4 l_p}{270L}\mathrm{Wi}^{*2} = 0, \tag{15}$$

which yields $\mu = \mathrm{Wi}^{*2/3}\sqrt[3]{\pi^4 l_p/(270L)}$ in the asymptotic limit $\mathrm{Wi}^* \to \infty$.

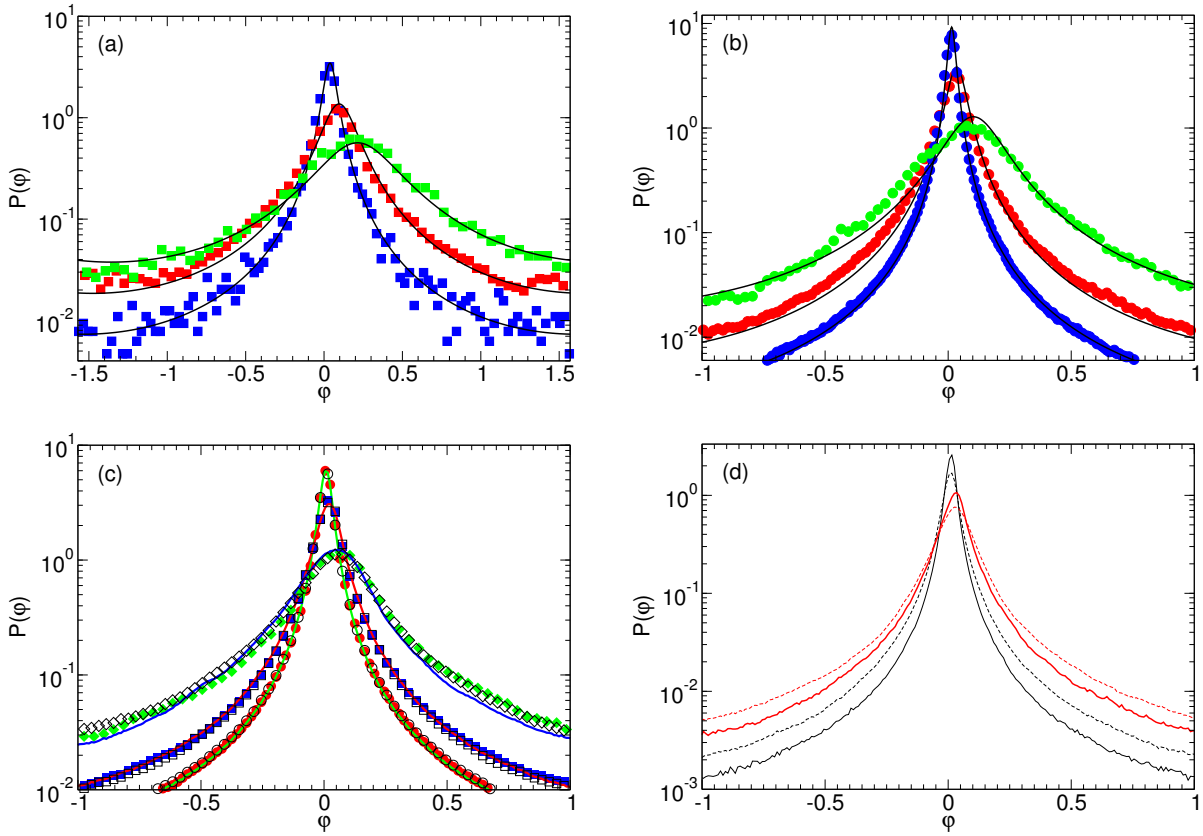

Figure 5. Probability distribution functions of the angle φ. (a) Dilute solution with $c/c^* = 0.16$ and $N_m = 50$ for $\mathrm{Wi_c} = 616.9$ (■), $\mathrm{Wi_c} = 61.7$ (■), and $\mathrm{Wi_c} = 12.3$ (■). (b) Dilute solution for $N_m = 250$, $c/c^* = 0.17$, and $\mathrm{Wi_c} = 2350$ (●), $\mathrm{Wi_c} = 235$ (●), $\mathrm{Wi_c} = 23.5$ (●). The solid lines in (a) and (b) are calculated according to Eq. (14) for the Weissenberg number $\mathrm{Wi}^* = \mathrm{Wi_c}/2$. (c) Semidilute solutions of polymers of length $N_m = 250$ for $c/c^* = 2.77$ with $\mathrm{Wi_c} = 5520$ (●), $\mathrm{Wi_c} = 552$ (■), and $\mathrm{Wi_c} = 55.2$ (♦), for $c/c^* = 5.19$ with $\mathrm{Wi_c} = 5423$ (○), $\mathrm{Wi_c} = 542.3$ (□), and $\mathrm{Wi_c} = 54.23$ (◇), as well as $c/c^* = 10.38$ with $\mathrm{Wi_c} = 5691$ (green line), $\mathrm{Wi_c} = 569.1$ (red line), $\mathrm{Wi_c} = 56.91$ (blue line). (d) Comparison of $P(\varphi)$ for dilute $c/c^* = 0.35$ (solid) and semidilute $c/c^* = 5.19$ (dashed) solutions with $\mathrm{Wi_c} = 2670$ (black solid line), $\mathrm{Wi_c} = 267$ (red solid line), $\mathrm{Wi_c} = 2700$ (black dashed line), and $\mathrm{Wi_c} = 270$ (red dashed line).

For a *dilute* solution, $P(\varphi)$ is shown in Figs. 5(a) and (b) for various Weissenberg numbers, together with theoretical lines obtained from Eq. (14) [11] (note that $\mathrm{Wi}^* = \mathrm{Wi_c}/2$). Evidently, the simulation results agree well with the analytical approach, as is expected for a dilute solution in which the intermolecular interactions are irrelevant. $P(\varphi)$ exhibits a significant shear-rate dependence. Without any shear, no angle is preferred. A finite shear rate leads to the appearance of a peak, which shifts to smaller values with increasing $\dot{\gamma}$ and, at the same time, the width $\Delta\varphi$ of $P(\varphi)$ decreases. Figure 5(c) displays distribution functions for various concentrations and Weissenberg numbers $\mathrm{Wi_c}$ of semidilute solutions. For every Weissenberg number, distributions are compared for three concentrations $c > c^*$. Evidently, the distributions are almost independent of concentration for the considered Weissenberg numbers. However, we observe a clear concentration dependence, when we compare distributions from dilute and semidilute solutions. Figure 5(d), displays distributions for the concentrations $c/c^* = 0.35$ and 5.19 and the Weissenberg numbers $\mathrm{Wi_c} \approx 267$, 2670 and 270, 2700, respectively. The increase

in concentration from a dilute solution beyond the overlap concentration leads to a broadening of the distribution function. Interestingly, the value φ_m at the peak of the distribution function is independent of concentration at a given $\mathrm{Wi_c}$ [18]. Theoretical calculations show that φ_m is close to the alignment angle χ_G [11].

6. Tumbling Dynamics

As has been shown [2, 18], the tumbling dynamics of a polymer can be characterized by and a characteristic time be obtained from the cross-correlation function

$$C_{xy}(t) = \frac{\left\langle G'_{xx}(t_0) G'_{yy}(t_0+t) \right\rangle}{\sqrt{\left\langle G'^2_{xx}(t_0) \right\rangle \left\langle G'^2_{yy}(t_0) \right\rangle}}, \tag{16}$$

for deviations from average stationary values $G'_{\beta\beta}(t) = G_{\beta\beta}(t) - \langle G_{\beta\beta} \rangle$ of the radius of gyration tensor components along the flow and gradient direction. Examples of cross-correlation functions are displayed in Fig. 6 for several shear rates and concentrations. Every curves exhibits a deep minimum at a time $t_+ > 0$ and a pronounced maximum at a time $t_- < 0$, and decays to zero at large time-lags. Hence, the tumbling dynamics is not periodic, but cyclic. The latter has been questioned for tethered polymers [26]. The minimum at t_+ indicates that positive values of $G'_{\beta\beta}$ are linked with negative ones of the orthogonal directions, i.e., polymer shrinkage in the y-direction is linked with its extension in x-direction, and similarly, an extension in y-direction is linked to shrinkage in x-direction. The maximum of $C_{xy}(t)$ reveals that positive deviations G'_{xx} are correlated with positive values G'_{yy} at earlier times, or a collapsed state along the x-direction ($G'_{xx} < 0$) is correlated with a previous collapsed state in y-direction [2]. Hence, the time difference $t_+ - t_-$ is related to conformational changes that a polymer undergoes during tumbling, which is characterized by the time $\tau_t = 2(t_+ - t_-)$ [2]. The factor two accounts for the fact that two non-equivalent conformations lead to a maximum and a minimum, respectively, and will be (more or less) assumed during a cycle.

As shown in Fig. 6, the positions of the maxima and minima are rather close for equal Weissenberg numbers, when the lag-time is scaled by the relaxation time $\tau(c)$. Hence, the tumbling times exhibit a strong concentration dependence due to the concentration dependence of the relaxation times [17].

Normalized tumbling frequencies $f = \tau(c)/\tau_T$, with tumbling times extracted from the correlation functions and scaled by the corresponding relaxation times $\tau(c)$, are presented in Fig. 6 (right) for a wide range of shear rates and concentrations. For comparison, the theoretical prediction for a polymer in dilute solution is presented as well [11, 16]. The results agree very well. The short chain results clearly show the crossover from unity, assumed in the limit $\dot{\gamma} \to 0$, to the asymptotic dependence $\sim \mathrm{Wi_c^{2/3}}$ at high shear rates. We obtain a chain-length dependence in close agreement with the theoretical prediction. More importantly, we find a slight and gradual shift of f to larger values with increasing concentration at a given $\mathrm{Wi_c}$, until a saturation is reached in the semidilute regime $c/c^* > 1$. This is seen for the two largest concentrations for $N_m = 50$ and the three largest ones for $N_m = 250$. As a consequence, the polymers exhibit a universal behavior, both in dilute ($c \ll c^*$) as well as in semidilute solution as function of $\mathrm{Wi_c}$, with the same power-law dependence on $\mathrm{Wi_c}$ (for $\mathrm{Wi_c} > 1$).

Alternatively, relaxation times under shear flow can be obtained by the end-to-end vector auto-correlation function $\langle R_\beta(t) R_\beta(0) \rangle$, where $R_\beta = R_{N_m,\beta} - R_{1,\beta}$ [10, 11, 28, 66, 67]. Similar to the results presented in Refs. [28, 66], we find a damped oscillatory behavior for $\mathrm{Wi_c} \gtrsim 1$ [67]. By fitting the obtained correlation function with the function

$$F_\beta(t) = a_\beta e^{-t/\tau_\beta^{(1)}} \left[\cos(\omega_\beta t) + b_\beta \sin(\omega_\beta t)\right] + [1 - a_\beta] e^{t/\tau_\beta^{(2)}}, \tag{17}$$

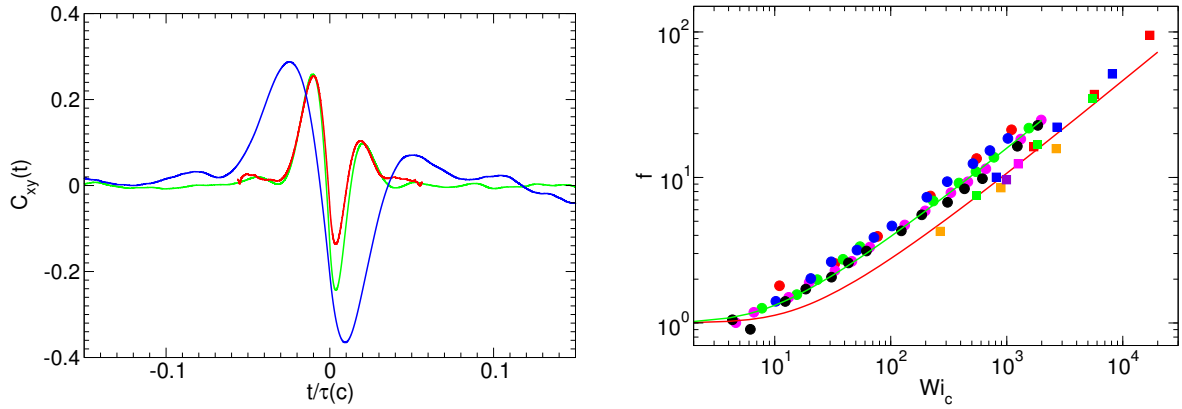

Figure 6. Left: Cross-correlation functions [Eq. (16)] for a polymer of length $N_m = 250$ and the concentrations $c/c^* = 2.77$ (green), $c/c^* = 10.38$, (red), and $c/c^* = 0.35$ (blue), corresponding to the Weissenberg numbers $\mathrm{Wi_c} = 5520$, $\mathrm{Wi_c} = 5690$, and $\mathrm{Wi_c} = 2670$, respectively. Right: Normalized tumbling frequencies $f = \tau(c)/\tau_T$. Bullets correspond to the polymer length $N_m = 50$ for $c/c^* = 0.16$ (●), $c/c^* = 0.41$ (●), $c/c^* = 0.81$ (●), $c/c^* = 1.63$ (●), and $c/c^* = 2.08$ (●). Squares indicate results for $N_m = 250$ and $c/c^* = 0.35$ (■), $c/c^* = 0.69$ (■), $c/c^* = 1.38$ (■), $c/c^* = 2.77$ (■), $c/c^* = 5.19$ (■), $c/c^* = 10.38$ (■). The lines present the theoretical predictions [11, 16].

with the amplitudes a_β, b_β, relaxation times $\tau_\beta^{(i)}$, and frequencies ω_β, we obtain non-equilibrium relaxation times. Strictly speaking, the functional form of the correlation function is unknown. As expressed by the correlation function C_{xy} (16), tumbling is non-periodic and, hence, Eq. (17) applies over a certain time window only. We expect the equation to capture correlations in the polymer conformations over a time scale comparable to a tumbling cycle.

By fitting, we obtain the following general relations for the various shear rates and densities: $a_x \approx a_z \approx 1$, $a_y \approx 1/2$, and $\omega_z = 0$, $\omega_x \approx \omega_y$. Since $a_y \approx 1/2$, the decay in the gradient direction is governed by two exponentials, where $\tau_y^{(2)}$ is an order of magnitude smaller than $\tau_y^{(1)}$, but shows a similar shear-rate dependence. Since $\omega_z = 0$, the correlation function along the vorticity direction decays exponentially. Moreover, b_x and b_y, where b_y is negative, are approximately independent of shear rate, but depend on polymer length. Most importantly, the relaxation times $\tau_x^{(1)}$, $\tau_y^{(1)}$, and $\tau_z^{(1)}$ are equal in dilute solution and agree with the tumbling times displayed in Fig. 6 (right). Hence, the polymer tumbling times are equal to the non-equilibrium end-to-end relaxation times. The parameter ω_β is independent of shear rate for the considered systems. This is in contrast to results of Ref. [66], where very short polymers ($N_m = 10$) have been considered only.

We attribute the concentration independence of the tumbling time and the probability distribution functions for $c/c^* > 1$ to screening of hydrodynamic interactions. To confirm our hypothesis, we performed Brownian MPC simulations for dilute and semidilute solutions [18]. Using similar Weissenberg numbers, we find, within the accuracy of the simulations, identical distribution functions $P(\varphi)$ for both cases. Moreover, the distributions agree with those of semidilute systems of the same concentration and Weissenberg number in the presence of hydrodynamic interactions. Hence, the differences between distribution functions at low and high concentrations, as displayed in Fig. 5(d), are due to hydrodynamic interactions. In dilute solutions, hydrodynamic interactions are present, whereas in systems with $c > c^*$, hydrodynamic interactions are screened. Naturally, at larger concentrations friction is higher. This aspect is

captured in the relaxation time $\tau(c)$, which increases considerably with concentration [17].

The fact that the tumbling frequencies and the widths of the distribution functions are larger in semidilute solutions, i.e., when hydrodynamic interactions are screened, might be explained as follows. (i) The observed broadening of the distribution function $P(\varphi)$ in semidilute solution implies that hydrodynamic interactions favor polymer alignment and lead to a faster dynamics during the collapse and stretching part of the tumbling motion. (ii) At the same Weissenberg number, the shear rate of a non-draining polymer is larger than that of a free-draining one, due to differences in equilibrium relaxation times, i.e., for a coiled conformation. As a consequence, the effective Weissenberg number $\mathrm{Wi}_R = \dot{\gamma}\tau_R$, where τ_R is the rotational relaxation time in the stretched rodlike conformation, of the non-draining polymer is larger than that of the free-draining one. This could explain the larger probability of angles in the vicinity of φ_m for non-draining polymers as well as their faster collapse dynamics. Overall, the tumbling time is larger in a non-draining system.

The broadening of the distribution functions with increasing concentration or screening of hydrodynamic interactions is not captured by standard theories employing the preaveraging approximation [11, 16, 21]. Here, hydrodynamic interactions are included in the relaxation times and hence the Weissenberg number only; additional, "higher order effects" are neglected. Therefore, one might expect that the theoretical description would reproduce results of simulations without hydrodynamic interactions. In contrast, the model calculations rather reproduce the simulation data for systems with hydrodynamic interactions.

7. Conclusions

We have calculated conformational, dynamical, and rheological properties of polymers in dilute and semidilute solution under shear flow by mesoscale hydrodynamic simulations. We find that their stationary-state conformational and rheological properties are independent of concentration when expressed in terms of the Weissenberg number $\mathrm{Wi}_\mathrm{c} = \dot{\gamma}\tau(c)$. This is remarkable, since the longest polymer relaxation time $\tau(c)$ increases significantly with concentration and indicates that an effective local friction determines the stationary-state properties.

By analyzing dynamical properties—orientational distribution functions and tumbling times—of semidilute polymer solutions, we find that they depend on concentration (in excess of $\tau(c)$), a dependence which we attribute to screening of hydrodynamic interactions in semidilute solution. Compared to the dilute case, such a screening causes a broadening of orientational angle distribution functions and an increasing ratio $f = \tau(c)/\tau_T$ at the same Weissenberg number Wi_c in semidilute solution. The effect itself is small ($f(c = 0)/f(c > c^*) \approx 1.3$ at $\mathrm{Wi}_\mathrm{c} = 10^3$). More importantly, the same asymptotic dependencies are obtained as function of the Weissenberg number Wi_c in dilute and semidilute solutions. This explains the previously obtained agreement of power spectral densities obtained from free-draining and non-draining computer simulations [2].

Moreover, we find that the tumbling times almost quantitatively agree with the non-equilibrium end-to-end vector relaxation times, which, hence, exhibit the asymptotic shear rate dependence $\sim \dot{\gamma}^{-2/3}$ for $\dot{\gamma} \to \infty$.

Our simulations reveal a complex interplay between shear rate, deformation, and intramolecular excluded-volume interactions, which is difficult to grasp by analytical theory.

Acknowledgments

Financial support by the Deutsche Forschungsgemeinschaft within SFB TR6 "Physics of Colloidal Dispersions in External Fields" is gratefully acknowledged. We are grateful to the Jülich Supercomputer Centre (JSC) for allocation of a special CPU-time grant.

References

[1] Smith D E, Babcock H P and Chu S 1999 *Science* **283** 1724
[2] Schroeder C M, Teixeira R E, Shaqfeh E S G and Chu S 2005 *Phys. Rev. Lett.* **95** 018301
[3] Teixeira R E, Babcock H P, Shaqfeh E S G and Chu S 2005 *Macromolecules* **38** 581
[4] Gerashchenko S and Steinberg V 2006 *Phys. Rev. Lett.* **96** 038304
[5] Doyle P S, Ladoux B and Viovy J L 2000 *Phys. Rev. Lett.* **84** 4769
[6] Celani A, Puliafito A and Turitsyn K 2005 *Europhys. Lett.* **70** 464
[7] Chertkov M, Kolokolov I, Lebedev A and Turitsyn K 2005 *J. Fluid. Mech.* **531** 251
[8] Puliafito A and Turitsyn K 2005 *Physica D* **211** 9
[9] Schroeder C M, Teixeira R E, Shaqfeh E S G and Chu S 2005 *Macromolecules* **38** 1967
[10] Delgado-Buscalioni R 2006 *Phys. Rev. Lett.* **96** 088303
[11] Winkler R G 2006 *Phys. Rev. Lett.* **97** 128301
[12] Winkler R G, Mussawisade K, Ripoll M and Gompper G 2004 *J. Phys.: Condens. Matter* **16** S3941–S3954
[13] Ripoll M, Winkler R G and Gompper G 2006 *Phys. Rev. Lett.* **96** 188302
[14] Aust C, Kröger M and Hess S 1999 *Macromolecules* **32** 5660
[15] Wang S Q 1990 *J. Chem. Phys.* **92** 7618
[16] Winkler R G 2010 *J. Chem. Phys.* **133** 164905
[17] Huang C C, Winkler R G, Sutmann G and Gompper G 2010 *Macromolecules* **43** 10107
[18] Huang C C, Sutmann G, Gompper G and Winkler R G 2011 *EPL* **93** 54004
[19] Babcock H P, Smith D E, Hur J S, Shaqfeh E S G and Chu S 2000 *Phys. Rev. Lett.* **85** 2018
[20] Hur J, Shaqfeh E S G, Babcock H P, Smith D E and Chu S 2001 *J. Rheol.* **45** 421
[21] Doi M and Edwards S F 1986 *The Theory of Polymer Dynamics* (Oxford: Clarendon Press)
[22] Kapral R 2008 *Adv. Chem. Phys.* **140** 89
[23] Gompper G, Ihle T, Kroll D M and Winkler R G 2009 *Adv. Polym. Sci.* **221** 1
[24] Bird R B, Hassager O, Armstrong R C and Curtiss C F 1987 *Dynamics of Polymeric Liquids* vol 2 (New York: John Wiley Sons)
[25] Öttinger H C 1996 *Stochastoic Processes in Polymeric Fluids* (Berlin: Springer)
[26] Zhang Y, Donev A, Weisgraber T, Alder B J, Graham M G and de Pablo J J 2009 *J. Chem. Phys.* **130** 234902
[27] Kobayashi H and Yamamoto R 2010 *Phys. Rev. E* **81** 041807
[28] Usabiaga F B and Delgado-Buscalioni R 2011 *Macromol. Theory Simul.* **20** 466
[29] Das D and Sabhapandit S 2008 *Phys. Rev. Lett.* **101** 188301
[30] Malevanets A and Kapral R 1999 *J. Chem. Phys.* **110** 8605
[31] Malevanets A and Kapral R 2000 *J. Chem. Phys.* **112** 7260–7269
[32] Malevanets A and Yeomans J M 2000 *Europhys. Lett.* **52** 231–237
[33] Ripoll M, Mussawisade K, Winkler R G and Gompper G 2004 *Europhys. Lett.* **68** 106
[34] Ripoll M, Mussawisade K, Winkler R G and Gompper G 2005 *Phys. Rev. E* **72** 016701
[35] Mussawisade K, Ripoll M, Winkler R G and Gompper G 2005 *J. Chem. Phys.* **123** 144905
[36] Padding J T and Louis A A 2006 *Phys. Rev. E* **73** 031402
[37] Ryder J F and Yeomans J M 2006 *J. Chem. Phys.* **125** 194906
[38] Cannavacciuolo L, Winkler R G and Gompper G 2008 *EPL* **83** 34007
[39] Frank S and Winkler R G 2008 *EPL* **83** 38004
[40] Chelakkot R, Winkler R G and Gompper G 2010 *EPL* **91** 14001
[41] Padding J T and Louis A A 2004 *Phys. Rev. Lett.* **93** 220601
[42] Wysocki A, Royall C P, Winkler R G, Gompper G, Tanaka H, van Blaaderen A and Löwen H 2009 *Soft Matter* **5** 1340
[43] Noguchi H and Gompper G 2004 *Phys. Rev. Lett.* **93** 258102
[44] Noguchi H and Gompper G 2005 *Proc. Natl. Acad. Sci. USA* **102** 14159–14164
[45] McWhirter J L, Noguchi H and Gompper G 2009 *Proc. Natl. Acad. Sci. USA* **106** 6039
[46] Galuschko A, Spirin L, Kreer T, Johner A, Pastorino C, Wittmer J and Baschnagel J 2010 *Langmuir* **26** 6418
[47] Allen M P and Tildesley D J 1987 *Computer Simulation of Liquids* (Oxford: Clarendon Press)
[48] Swope W C, Andersen H C, Berens P H and Wilson K R 1982 *J. Chem. Phys.* **76** 637
[49] Ihle T and Kroll D M 2001 *Phys. Rev. E* **63** 020201(R)
[50] Winkler R G and Huang C C 2009 *J. Chem. Phys.* **130** 074907
[51] Huang C C, Chatterji A, Sutmann G, Gompper G and Winkler R G 2010 *J. Comput. Phys.* **229** 168
[52] Sutmann G, Huang C C, Winkler R G and Gompper G 2010 *John von Neumann Institute for Computing NIC Symposium 2010* (*IAS Series* vol 3) ed Münster G, Wolf D and Kremer M (Jülich: Forschungszentrum Jülich) pp 287–294

[53] Ripoll M, Winkler R G and Gompper G 2007 *Eur. Phys. J. E* **23** 349
[54] Bruns W and Carl W 1993 *Macromolecules* **26** 557
[55] Carl W and Bruns W 1994 *Macromol. Theory Simul.* **3** 295
[56] Pierleoni C and Ryckaert J P 1995 *Macromolecules* **28** 5097
[57] Lindner P and Oberthur R C 1988 *Colloid Polym. Sci.* **266** 886
[58] Lindner P and Oberthur R C 1989 *Physica B* **156 & 157** 410
[59] Bird R B, Armstrong R C and Hassager O 1976 *Dynamics of Polymeric Liquids* vol 1 (New York: Wiley)
[60] Winkler R G, Morawitz M and Yoon D Y 1992 *Mol. Phys.* **75** 669
[61] Liu T W 1989 *J. Chem. Phys.* **90** 5826
[62] Petera D and Muthukumar M 1999 *J. Chem. Phys.* **111** 7614
[63] Hsieh C C and Larson R G 2004 *J. Rheol.* **48** 995
[64] Rubinstein M and Colby R 2003 *Polymer Physics* (Oxford: Oxford University Press)
[65] Zylka W 1991 *J. Chem. Phys.* **94** 4628
[66] Jose P P and Szamel G 2008 *J. Chem. Phys.* **128** 224910
[67] Haung C C, Gompper G and Winkler R G 20012 submitted for publication